Pumpless Loop for Narrow Channel and Micro-Channel Boiling

Swaraj Mukherjee

Issam Mudawar

Purdue University International Electronic Cooling Alliance (PUIECA), West Lafayette, IN 47907

A compact cooling system is examined which capitalizes upon fluid density differences between two vertical, parallel, interconnected tubes to achieve a pumpless cooling loop. A heat-dissipating device is incorporated into a boiler at the bottom of the hot tube. The large density differences between the two tubes produces a substantial nonequilibrium in hydrostatic pressure, drawing liquid downwards through the cold tube as a two-phase mixture is released upwards in the hot tube. Cooling with this pumpless loop is fundamentally different from, and far superior to, pool boiling thermosyphons because of the former's ability to separate the path of replenishment liquid from that of the released vapor. Experiments were performed to explore the effects of boiler gap (separation distance between the boiling surface and opposite insulating wall) on cooling performance and critical heat flux (CHF) for water and FC-72. The gap, which is the primary measure of boiler miniaturization, was varied from 0.051 to 21.46 mm. For large gaps, CHF showed insignificant dependence on the gap for both fluids. However, small gaps produced CHF variations that were both drastic and which followed opposite trends for the two fluids. Decreasing the gap below 3.56 mm produced a substantial rise in CHF for FC-72. For water, CHF was fairly insensitive down to 0.51 mm, below which it began to decrease sharply. These trends are shown to be closely related to the small surface tension and contact angle of FC-72 producing very small bubbles which can easily pass through narrow gaps in FC-72, while much larger bubbles in water obstruct liquid replenishment in narrow gaps. A numerical model is constructed to determine how the gap influences the various components of pressure drop, velocities, coolant flow rate, and hence system response to heat input. [DOI: 10.1115/1.1602708]

Introduction

Several cooling schemes have been developed in recent years to combat the large increases in heat dissipation from electronic and power devices. Air-cooled heat sinks are presently found in most personal computers, but are rapidly approaching accepted industry limits for noise and vibration. In addition, the poor thermal path between the device and air stream produces unacceptably high device temperatures when dissipating high heat fluxes. Liquid cooling can alleviate those concerns by greatly reducing the thermal resistance between the device and coolant, especially when the device is fully submerged in the coolant. The heat is dissipated first to the coolant and ultimately rejected to an air stream via a remote high-performance heat exchanger.

Liquid cooling can be implemented in a broad range of configurations, including natural convection, channel flow, jet-impingement, and spray cooling. There is ample evidence that phase change of a liquid coolant greatly enhances cooling performance relative to single-phase systems [1]. Two types of liquid coolants are commonly used for dissipation of concentrated heat loads. Water is inexpensive, widely available, and possesses very attractive thermal transport properties. However, its poor dielectric properties preclude its use in intimate contact with current-carrying components. Hence water is used only in indirect cooling configurations, buffered from electrical components, and where extremely high heat fluxes are encountered, such as in fusion reactor blankets [2,3] and x-ray devices [4]. The other type of coolant are fluorochemical liquids that are available with a broad range of boiling points to suit different cooling needs. They include DuPont's Freon refrigerants and 3M's Fluorinerts. The latter are a family of chlorine-free liquid coolants that have unprecedented dielectric properties, making them ideal candidates for direct-immersion cooling of electronic devices. Unfortunately, their thermal transport properties are far inferior to those of water, which greatly compromises their cooling effectiveness.

Micro-cooling devices are especially popular because their small size is well suited for electronic devices, let alone their miniscule coolant inventory requirements. Liquid flow in micro-coolers is typically laminar, which results in a heat transfer coefficient inversely proportional to the hydraulic diameter. Thus enormous heat transfer coefficients can be realized simply by reducing hydraulic diameter [5]. Unfortunately, micro-cooling devices are known to produce enormous pressure drop when dissipating high heat fluxes. They are also plagued by large stream-wise temperature increases in both the coolant and the heat-dissipating device. Those increases are often detrimental to temperature-sensitive devices such as computer processors.

By allowing partial or total consumption of the liquid coolant by boiling, two-phase micro-channel coolers can greatly reduce coolant flow rate requirements relative to single-phase systems [6]. They also help maintain stream-wise temperature uniformity by capitalizing on latent, rather than sensible heat transfer. But like single-phase micro-channel coolers, they can produce excessive pressure drop when dissipating high heat fluxes. Much attention is now being focused on the development of micro-pumps for miniature cooling loops. Thus far, micro-pumps have failed to deliver adequate coolant flow rates, and their reliability remains illusive.

Ironically, the increase in electronic device heat dissipation, which is requiring increasingly complex cooling solutions, is taking place as the computer industry is facing shrinking profit margins and pricing pressures. Cost alone has precluded the deployment of several highly effective liquid cooling schemes, including

Contributed by the Electronic and Photonic Packaging Division for publication in the JOURNAL OF ELECTRONIC PACKAGING. Manuscript received June 2002. Associate Editor: B. Courtois.

jet-impingement and sprays. What the industry is presently after are liquid cooling schemes that are thermally effective, reliable, compact, and low cost.

Heat pipes, which are presently used in notebook computers, do satisfy the size, cost, and reliability requirements. However, it is widely acknowledged in the computer industry that heat pipes are no longer able to handle anticipated heat dissipation requirements of advanced processors. A key limitation of heat pipes is the miniscule liquid flow rate possible with capillary forces. Thermosyphons are better suited where gravity can be effectively utilized within the confines of an electronic housing. The heat-dissipating device is submerged in a boiler, where pool boiling releases vapor that rises by buoyancy to an elevated air-cooled condenser, returns to liquid state, and drips back to the boiler below. Thermosyphons are far less expensive than other cooling schemes because they are pumpless, self-contained, and therefore maintenance free. Two key thermal limitations of thermosyphons utilizing dielectric coolants are incipient boiling temperature drop and relatively low critical heat flux (CHF) [7]. The incipient boiling temperature drop is the result of the low contact angle of dielectric coolants enabling the liquid to flood surface cavities, precluding the capture of large vapor embryos. The few small embryos remaining in cavities require unusually high surface temperatures to nucleate. But once a cavity begins to nucleate, vapor is deposited into neighboring cavities, which are quickly activated as well. A nucleation front propagates very rapidly across the surface. In the process, an appreciable fraction of the surface undergoes a sudden transformation from single-phase natural convection to nucleate boiling, resulting in a large temperature drop and potential damage to the device by thermal shock.

The second obvious limitation of thermosyphons is the relatively low CHF associated with pool boiling. A single occurrence of the sudden, unsteady rise in surface temperature associated with CHF can lead to permanent device damage. Without surface augmentation, the Zuber et al. model [8] predicts that CHF for saturated pool boiling in FC-72 is $15.24\ \mathrm{W\,cm^{-2}}$ and $110.4\ \mathrm{W\,cm^{-2}}$ in water. However, these predictions assume an infinite pool of liquid. The geometrical confines of the miniature boiler required for electronic cooling are likely to interrupt liquid replenishment of the device surface during vigorous boiling, hence greatly compromising CHF from the above indicated values.

This paper explores a new cooling system specifically tailored to compact, high-flux electronic cooling systems. Key design requirements of this new concept are (1) pumpless coolant circulation, (2) cooling effectiveness, (3) compactness, (4) reliability, (5) maintenance-free operation, (6) use of a dielectric coolant, and (7) low cost. This new cooling system is also intended to circumvent the thermal limitations of its thermosyphon predecessor, namely, incipient boiling temperature drop and low CHF.

Pumpless Loop Cooling Concept. The system examined in this paper utilizes fluid density differences between two vertical, parallel tubes to achieve coolant flow. As shown in Fig. 1, the two tubes are connected at the top to a free-surface reservoir, which is connected to a condenser above, and the heat dissipating device is incorporated into a boiler in one of the tubes, the ''hot tube.'' The principle involved is that when liquid in the hot tube is heated beyond the saturation temperature, bubbles will form which are driven upwards by buoyancy. The vapor production greatly decreases the mixture density in the hot tube, while the other ''cold tube'' maintains a fairly constant liquid density. The large fluid density differences between the two tubes produces a substantial nonequilibrium in hydrostatic pressure which, in the presence of a free interface in the reservoir, produces a higher pressure at the bottom of the cold tube compared to the hot tube. This sets up a clockwise cooling circuit, where liquid is drawn downwards from the reservoir through the cold tube as a two-phase mixture is released upwards in the hot tube. Once the cooling circuit is set into motion, the coolant flow will adjust itself in response to the

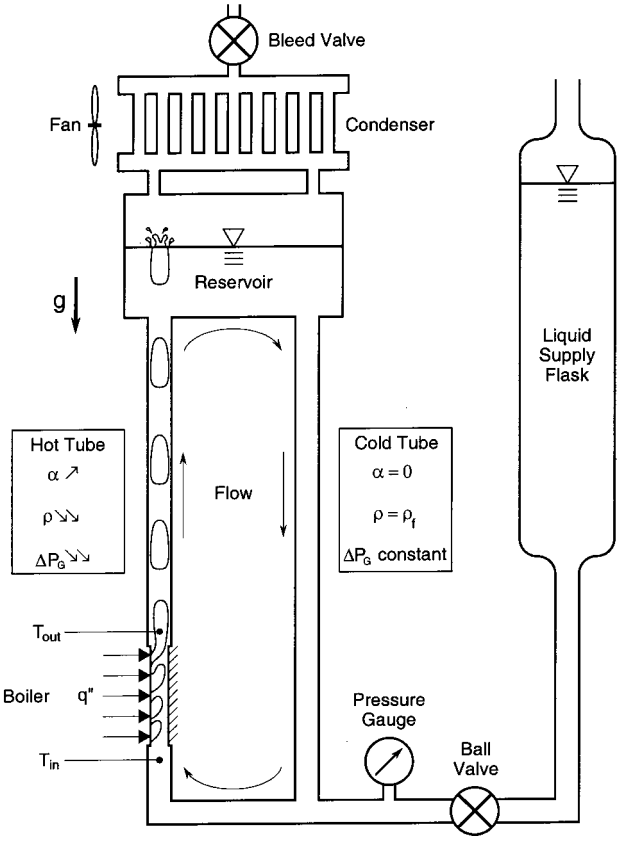

Fig. 1 Pumpless loop cooling concept and experimental setup

complex gravitational (density driven), frictional, and accelerational pressure drop interactions, dictated solely by the heat input to the hot tube. Cooling with this pumpless loop is fundamentally different from pool boiling thermosyphons. The latter relies on liquid penetration between departing vapor masses to replenish the heated surface, and any reduction in the size of the liquid pool can interrupt the liquid replenishment. The present pumpless loop concept completely separates the path of the replenishment liquid from that of the released vapor.

Interestingly, the concept of coolant flow between cold and hot parallel tubes is by no means new. For example, it is encountered in the boilers of conventional power generation plants [9]. Many boiler designs consist of a large number of vertical parallel tube bundles that carry water between two large headers, and heat released from the combustion process boils the water gradually along each tube. Lack of uniformity in the combustion process results in some (cold) tubes receiving less heat than the other (hot) tubes. This creates appreciable two-phase density gradients between tubes, which often leads to downflow in the cold tubes. This phenomenon is highly undesirable in power plants, and several control measures are adopted to prevent it, since it can greatly compromise cycle efficiency. The same form of instability is used *advantageously* in the present system to set up the desired cooling loop. The present pumpless loop concept also capitalizes upon the heat transfer augmentation effects of flow boiling in narrow gaps.

The present cooling concept constitutes a ''smart,'' self-driven system. The term smart is used to designate a class of systems that can respond passively to enhance performance without external control input, such as a variable speed pump, to respond to the heat input. As the heat input increases in the present system, coolant flow is initiated by density differences between the cold and hot tubes. For small boiler gaps, increasing heat input increases the void fraction in the hot tube, which both increases the density

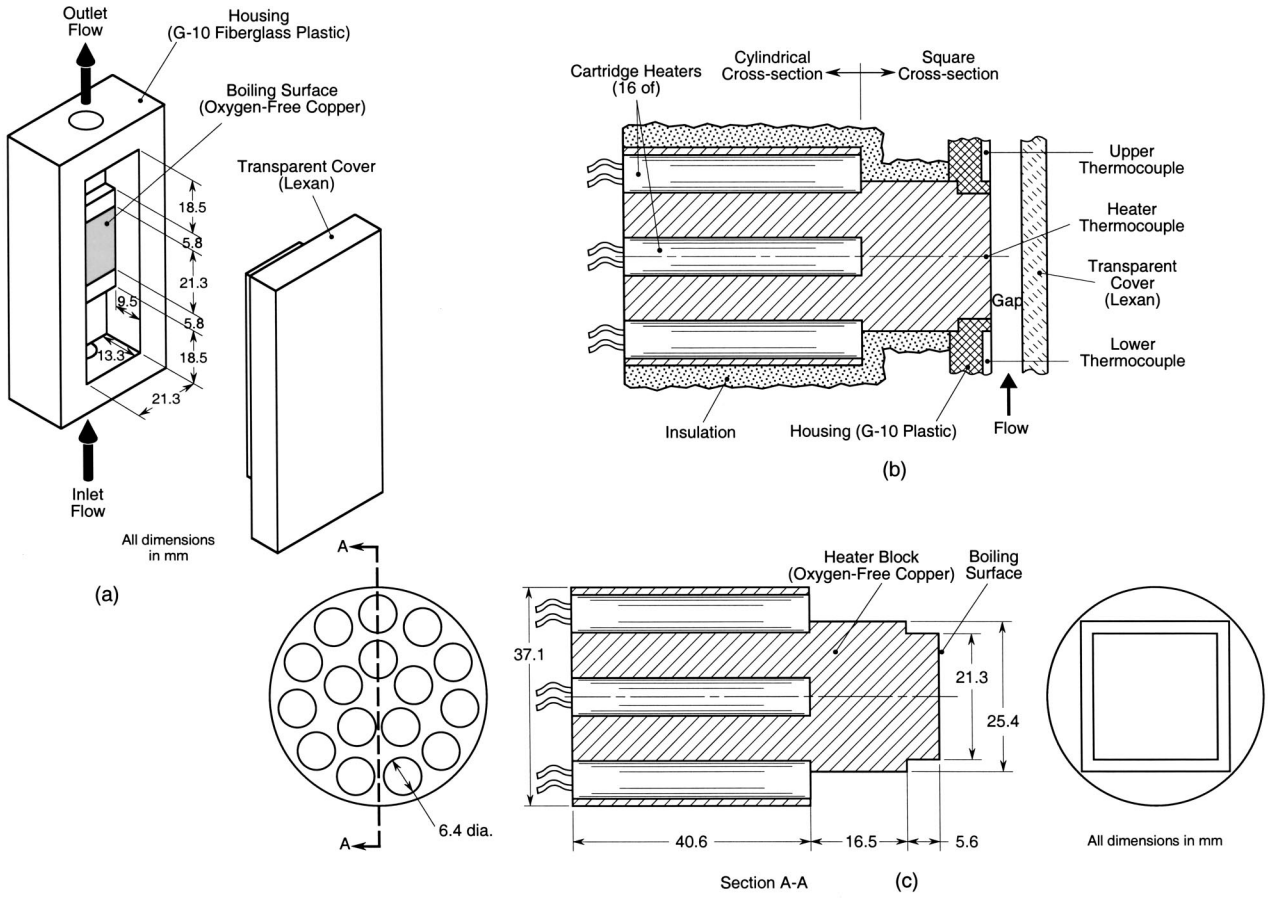

Fig. 2 Details of (*a*) housing, (*b*) sectional view, and (*c*) heater of test module

difference between the two tubes, and the velocity of the two-phase mixture within the boiler, thereby increasing the cooling capacity even more.

In this paper, the performance of this pumpless cooling system is explored and compared for FC-72 and water. Experiments were performed to (a) demonstrate the validity of the concept, (b) visualize the vapor-liquid interactions for FC-72 and water, and (c) examine the influence of boiler gap (key miniaturization parameter) on cooling performance. A numerical model is then constructed to determine how the boiler gap influences the various components of pressure drop, velocities, and coolant flow rate in the cooling loop, and hence system response to heat input.

Experimental Facility and Methods

Test Module. As shown in Fig. 2(*a*), the test module consisted of a rectangular G-10 fiberglass plastic housing, to which a vertical heated surface was attached, and a transparent cover plate. The square boiling surface was flush mounted in a raised platform in the cavity of the housing. The primary purpose of the raised platform was to produce a step in the flow, ensuring a fair degree of turbulence in the liquid prior to flowing over the boiling surface. Constructed from optically clear polycarbonate plastic (Lexan), the cover was designed to vary the flow gap between the boiling surface and cover. An O ring around the perimeter of the housing prevented any leakage from the module cavity. The interface between the housing and the square shoulder of the heater was sealed off with high-temperature silicone rubber.

Since the depth of the boiling surface was 9.5 mm from the housing surface (see Fig. 2(*a*)), the gap could be either increased or decreased according to how the cover was machined. A separate cover plate was fabricated for each gap of less than 9.5 mm. Those cover plates where machined with a projecting face, the depth of the projection corresponded to the desired decrease from 9.5 mm. For flow gaps greater than 9.5 mm, the cover plate consisted of a universal cover plate fitted with a spacer that provided the required increase in thickness above 9.5 mm. Coolant leaks between the cover plate and spacer were prevented by an O ring. A total of 13 polycarbonate cover combinations were machined, providing gaps ranging from 0.051 to 21.46 mm.

Figure 2(*b*) shows a sectional view of the test module, including the detailed construction of the test heater. The square boiling surface exposed to the coolant simulated a computer processor or other high heat flux source. The boiling surface was lapped after machining to ensure complete flatness and smoothness. The heating block was fabricated from high purity oxygen-free copper, which was square along the coolant side and cylindrical on the opposite end. A shoulder in the square portion allowed a snug fit with the G-10 housing. As shown in Fig. 2(*c*), the cylindrical portion contained 16 Hotwatt cartridge heaters rated to dissipate up to 120 W at 120 V each.

Three K-type thermocouples were used to measure the thermal performance of the system. One was inserted into the heater block just beneath the boiling surface, and from which the boiling surface temperature was determined. The other two were inserted into the coolant flow from the side of the boiler housing. One measured the liquid temperature at inlet to the boiling surface (which was close to the liquid saturation temperature), while the other measured the temperature of the two phase mixture just emerging from the boiling surface.

System Hardware. As shown in Fig. 1, the test module was connected to the reservoir via both the hot and cold tubes. Any vapor produced in the hot tube simply bubbled through the reser-

Table 1 Geometrical parameters of study

Parameter		Parameter	
L_1	0.45 m	d	0.00635 m
L_2	0.06 m	L	0.0213 m
L_3	0.04 m	A_s	0.000455 m^2
H	0.05 m		

voir liquid, and was released to a fan-cooled Lytron condenser. The condenser was situated directly above the reservoir, where the vapor condensed to liquid that dripped back into the reservoir. The condenser was bled to the atmosphere by means of a ball valve, which was kept slightly open to maintain atmospheric pressure at the free interface of the reservoir. A tee junction at the lowest point of the cold tube led to a liquid supply flask. The flask provided a pre-calibrated mass of coolant into the cooling loop before the flask was sealed off using a ball valve. A pressure gauge was connected to the lowest point of the cold tube in the liquid supply flask line. The hot and cold tubes were constructed of translucent PTFE tubing and connected to the other components of the apparatus via brass compression fittings. Table 1 lists all the key geometrical parameters of the test apparatus.

A Hewlett Packard 3497A data acquisition/control unit, interfaced to a Dell PC, was used for reading the three boiler module temperatures using Labview software. The test apparatus included two 12-amp, 0–140-V Staco variacs. One variac was used to modulate power feed to the cartridge heaters, and the other the condenser fan. A Yokogawa WT 200 digital power meter, with a precision of 0.02 percent, measured the power supply to the cartridge heaters.

Pictures were taken using a Nikon FM-2 camera with an assortment of close-up lenses. A continuous high-intensity light source or a strobe flash from a 1538A Strobotac were used for illumination, depending on bubble size, velocity, and coolant.

Experimental Procedure. The hot and cold tubes were first filled with liquid from the supply flask until the reservoir was partially filled with liquid. The supply flask ball valve was then closed and condenser fan switched on with the condenser valve slightly open. Power was supplied to the heater in small increments and measured by the power meter. The waiting period to ensure that the boiling surface temperature reached steady state varied according to heat flux at which the reading was being taken. In general, the waiting period for FC-72 and heat fluxes below 35 percent CHF varied from 30 to 85 min, decreasing to 5 min near CHF. The waiting period was shorter with water than with FC-72, given the superior thermal transport properties of the former. The power was switched off once CHF was detected.

Repeatability of the data was confirmed by performing three separate tests for select gaps. CHF values were repeatable to within 2.2 percent for FC-72 and 1.6 percent for water. The accuracy in measuring the boiler temperatures was better than 1°C. Heat loss from the heater to the surroundings was less than 2 percent of the supplied electrical power.

Results and Discussion

Experiments were carried out on a flat vertical boiling surface using water and FC-72. These two fluids possess drastically different thermophysical properties, as indicated in Table 2 for saturated conditions at one atmosphere. Most notably, both the latent heat of vaporization and surface tension are one order of magnitude greater for water than for FC-72. Additionally, FC-72 is known to produce vanishingly small contact angles (less than 1 deg) with most surfaces, compared to much greater contact angles for water that are sensitive to both surface material and surface finish.

All experiments were performed at atmospheric pressure and saturated conditions. Tests were performed to explore boiling conditions over a broad range of heat fluxes up to CHF for different gaps. Tests were also performed with a select number of gaps to capture bubble formation, coalescence, and departure at different heat fluxes in pursuit of a mechanistic understanding of the differences in boiling behavior between the two fluids.

Table 2 Thermophysical properties of saturated FC-72 and water at one atmosphere

Parameter	Water	FC-72
ρ_g	0.59 kg/m^3	13.13 kg/m^3
ρ_f	958.4 kg/m^3	1594 kg/m^3
ν_g	1.69 m^3/kg	0.0762 m^3/kg
ν_f	0.0014 m^3/kg	0.000627 m^3/kg
ν_{fg}	1.693 m^3/kg	0.0755341 m^3/kg
h_{fg}	2,257,900 J/kg	95,020 J/kg
μ_f	0.000279 N s/m^2	0.000436 N s/m^2
σ	0.0589 N/m	0.00841 N/m

Experimental Results. A total of 13 gaps were tested in FC-72 and 12 in water. These gaps ranged from 0.051 to 21.46 mm. Figures 3(*a*) and (*b*) show the variation of CHF with boiler gap for FC-72 and water, respectively. Overall, CHF values for FC-72 were smaller than for water because of the relatively poor thermophysical properties of the former. For relatively large gaps, CHF showed insignificant dependence on boiler gap for both fluids. However, small gaps produced changes in CHF that were both drastic and followed opposite trends for the two fluids. Decreasing the gap below 3.56 mm produced a substantial rise in CHF for FC-72, reaching a maximum for $\delta = 0.13$ mm, before beginning to decrease for smaller gaps. For water, CHF was fairly insensitive down to 0.51 mm, below which it began to decrease sharply.

Figures 4(*a*) and (*b*) show boiling curves for three representative gaps for FC-72 and water, respectively. Remarkably, the boiling curves for FC-72 show no signs of the incipience temperature drop commonly encountered in pool boiling systems [7]. The boiling curves for each fluid overlap in both the single-phase region and lower portion of the nucleate boiling region, leading to a

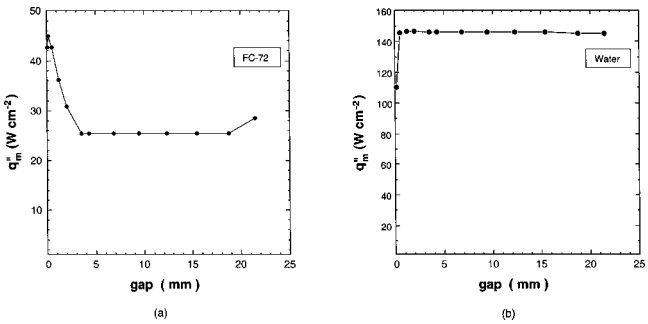

Fig. 3 CHF variation with boiler gap for (*a*) FC-72 and (*b*) water

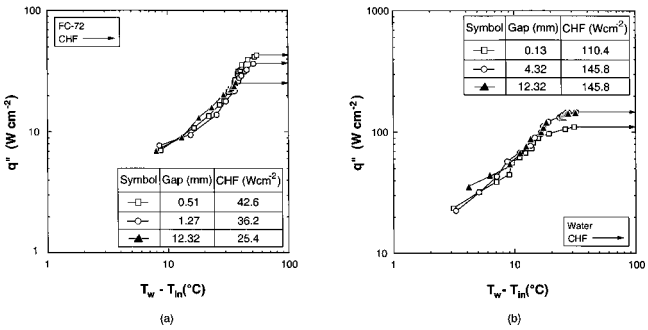

Fig. 4 Boiling curves for different gaps for (*a*) FC-72 and (*b*) water

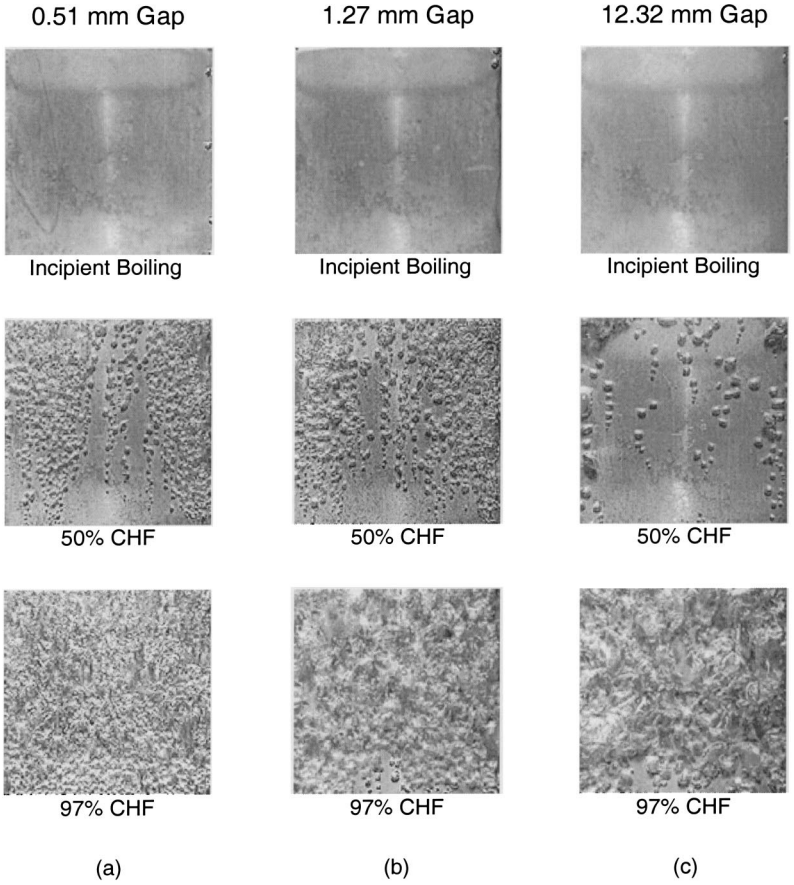

Fig. 5 Photos of boiling surface in FC-72 at different heat fluxes for (*a*) 0.51 mm, (*b*) 1.27 mm, and (*c*) 12.32-mm gap

different CHF value for each gap. Close inspection of the FC-72 boiling curves reveals a few degree enhancement in the nucleate boiling region for $\delta = 0.51$ mm relative to 1.27 mm. In what follows, photos of the boiling surface are discussed for different heat fluxes and representative gaps to help explain the unusual CHF trends.

Figures $5(a)-(c)$ show for all three gaps boiling commences along the vertical edges of the boiling surface. At these conditions, fluid motion is dominated by temperature-induced gradients in the liquid density. The liquid motion is highest near the middle of the boiling surface and suppressed near the vertical edges. This leads to both warmer fluid and weaker drag forces along the edges, conditions that are favorable for early bubble nucleation. At 50 percent CHF, Figs. $5(a)$ and (b) show vertical isolated columns of vapor forming towards the middle of the surface, where liquid velocity is highest, while more crowding of vapor columns is evident near the vertical edges. Interestingly, even with a small gap of 0.51 mm, bubbles at 50 percent CHF still could grow to their departure size without interacting with the transparent cover. Visual observation confirmed that these vertical columns started forming at about 30 percent CHF. More columns were generated at higher fluxes until 70 percent CHF, when the proliferation of bubbles columns along the entire surface both precluded the formation of any additional columns and signaled the onset of coalescence of bubbles from adjacent columns. At 97 percent CHF, small bubbles formed along the upstream (lower) edge of the surface for all three gaps. These bubbles coalesced downstream into larger bubbles whose size increased appreciably for larger gaps.

Figures $6(a)-(c)$ depict boiling behavior for water corresponding to three representative gaps. For the 0.13-mm gap, Fig. $6(a)$, a large number of bubbles emerged from the surface simultaneously at incipient boiling. A few groups of neighboring bubbles quickly coalesced into larger bubbles that spread laterally after making contact with the transparent cover. The enormous lateral growth of these large bubbles at 50 percent and 97 percent CHF greatly inhibited liquid replenishment for small gaps, which reduced CHF relative to larger gaps. For the two larger gaps, Figs. $6(a)$ and (b), no appreciable contact with the transparent cover occurred; bubbles coalesced locally and grew normal to the surface rather than spread laterally. CHF values therefore remained fairly constant for gaps greater than 0.51 mm. Comparing incipient boiling conditions for the three gaps shows bubble size increased with increasing gap. In general, the bubbles formed in water were uniformly distributed over the boiling surface, while bubbles in FC-72 followed preferential paths.

For both fluids, the two-phase mixture exiting the boiler exhibited a periodicity that was more easily distinguishable in water than in FC-72 due to the much larger size of bubbles generated in water. The period of vapor release decreased with increasing heat flux, becoming barely noticeable at very high fluxes as the vapor release became fairly continuous.

Figure $7(a)$ shows temporal plots of the boiling module temperatures at CHF$-$ (condition leading to CHF) in FC-72 for three gaps. These temperatures include the boiling surface temperature, T_w, the inlet fluid temperature below the boiling surface, T_{in}, and the outlet fluid temperature above the boiling surface, T_{out}. For the smallest gap of 0.51 mm, Fig. $7(a)$ shows cyclical temperature fluctuations in all three temperatures. The three temperatures increased very slowly until a short, rapid increase in T_w (about 0.2°C) occurred, following which the three temperatures dropped sharply in unison before repeating the thermal cycle once again. The cyclical temperature drops coincided with cyclical drops in

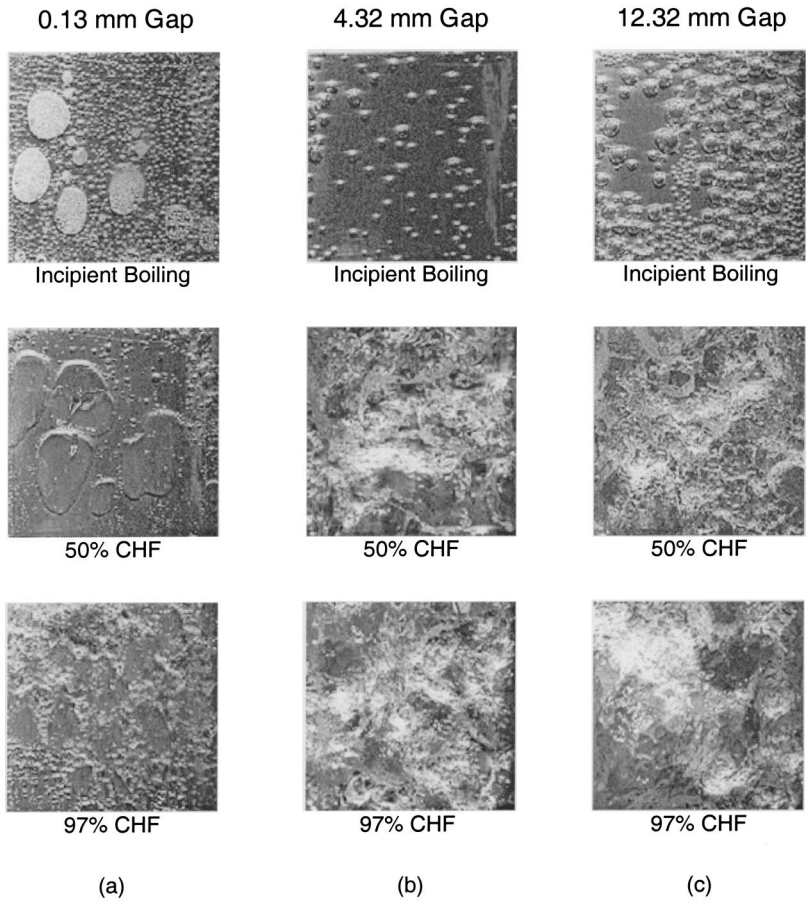

Fig. 6 Photos of boiling surface in water at different heat fluxes for (*a*) 0.13 mm, (*b*) 4.32 mm, and (*c*) 12.32-mm gap

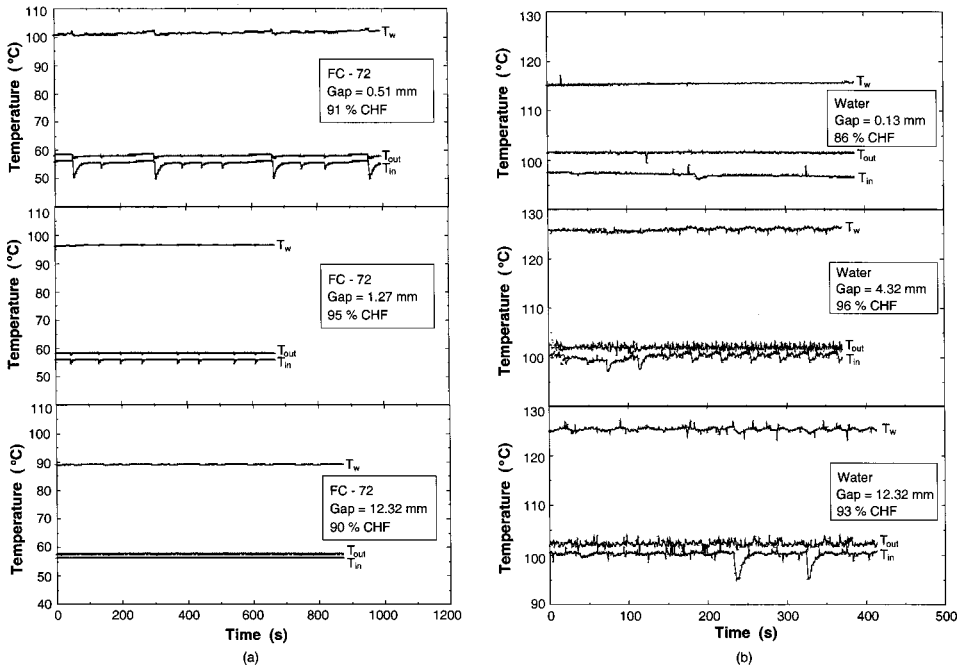

Fig. 7 Temporal records of boiler temperatures at CHF− for different gaps for (*a*) FC-72 and (*b*) water

Table 3 Bubble departure diameter for FC-72 and water based on the Fritz correlation [10]

	Contact angle, θ (in degrees)	d_b (mm)
FC-72	1	0.015
Water	50	2.60
	70	3.64
	90	4.68

the reservoir liquid level (explained below), which was more pronounced with smaller gaps, and virtually nonexistent for all gaps exceeding 3 mm. Interestingly, this cyclical drop was observed only as CHF was approached. Figure 7(a) shows a dampening of temperature drop with increasing gap; cycling was virtually nonexistent for $\delta = 12.32$ mm. Thermal cycling for the 0.51-mm gap consisted of high-frequency excursions superimposed on more dominant, large frequency drops.

One peculiarity about FC-72 was the fluctuation of liquid level in the reservoir above 70 percent CHF; liquid level was fairly constant below this heat flux. This was not sporadic but occurred at regular intervals, synchronous with the boiler inlet temperature variations indicated in Fig. 7(a). This phenomenon was not easily discernible with water.

At high heat fluxes, the liquid level in the reservoir started dropping steadily in FC-72 as the inlet temperature increased. The liquid dropped to its minimum level near the bottom of the reservoir just as the inlet temperature reached a maximum. The drop in liquid level was marred by slight fluctuations concurrent with the smaller ripples in the inlet temperature. The level remained steady for the next 20–70 s as the inlet temperature began to drop. The liquid then began to rise quickly to its initial level once the inlet temperature recovered from its drop. Interestingly, the temperature of the boiling surface exhibited negligible cycling for all heat fluxes below 90 percent CHF. As the flux was increased further, the period of fluctuation in both inlet temperature and liquid level started to diminish. However, the lowest liquid level in the reservoir remained constant irrespective of heat flux, and was impervious to the initial liquid level, as long as the reservoir was initially at least half full.

Figure 7(b) shows temporal plots of the boiling module temperatures for water. Comparing those with the FC-72 temporal plots, Fig. 7(a), shows cyclical temperature changes occurred with water as well, albeit with far less uniformity. More importantly, both the thermal cycling and reservoir liquid level fluctuations were far more pronounced for the larger gaps in water but smaller gaps in FC-72. This again points to drastically different behavior for the two fluids.

These unusual trends seem to be closely related to bubble departure diameter. The vast differences in both surface tension and contact angle between the two fluids (both properties being much smaller for FC-72 than for water) produce much smaller bubbles in FC-72. Table 2 shows the surface tension of water is seven times that of FC-72. In addition, FC-72 is a highly wetting fluid, maintaining a contact angle of less than one degree with most surface materials and finishes [7]. Table 3 shows the drastic differences between the bubble departure diameters for FC-72 and water according to the Fritz Bond number correlation [10],

$$Bo \equiv \frac{g(\rho_f - \rho_g)d_b^2}{\sigma} = 4.33 \times 10^{-4} \quad \theta^2, \tag{1}$$

where θ is the contact angle in degrees. A contact angle of 1° is assumed for FC-72 compared to a range of 50–90° for water, which is known to have high sensitivity to both surface material and surface finish.

The small departure diameter in FC-72 means bubbles will remain in close proximity to the surface, allowing replenishment liquid to flow unobstructed even in very small gaps. On the other hand, vapor bubbles in water are several orders of magnitude greater, meaning for small gaps they will grow and interact with the transparent cover before spreading laterally to fill a significant portion of the area available for the replenishment liquid flow. CHF is therefore greatly compromised in water for small gaps.

While the bubble diameter values in Table 3 help explain why small gaps greatly decrease CHF for water and not for FC-72, this simple bubble departure criterion does not explain why CHF increases appreciably in FC-72 with decreasing gap (excepting extremely small gaps below 0.13 mm). Recall that the present system sets up a flow loop, with liquid constantly reentering the boiler to compensate for the two-phase mixture being released upward from the boiler. Comparing the drag force exerted by the liquid flow on a bubble and the surface tension force responsible for bubble attachment to the surface proves the departure diameter in flow boiling is inversely proportional to the square of liquid velocity. Decreasing flow gap will increase flow velocity, which reduces both the departure diameter and the flow blockage due to the bubbles. Hence CHF increases in FC-72 with decreasing gap. This enhancement is possible until the gap is less than a critical value, at which point flow blockage will occur even in FC-72 and CHF begins decreasing. This is precisely what is observed in Fig. 3(a).

The enhancement effect resulting from decreasing the gap is not realized in water since the increase in liquid velocity is apparently too weak to clear the bubbles obstructing the liquid replenishment. Figure 6(b) shows CHF for water decreases significantly starting at a gap of 0.13 mm. This is due to the fact that the water bubbles cannot form freely and are impeded by smaller gaps. This is quite apparent in Fig. 6(a), where, even at incipient boiling, a significant number of bubbles are being squeezed by the transparent cover.

To illustrate the merits of the pumpless loop relative to pool boiling, the experimental apparatus was modified by disconnecting the cold tube entirely, reducing the system to a simple pool boiling thermosyphon. Table 4 compares the measured pool boil-

Table 4 Comparison of measured CHF for pumpless loop and pool boiling for FC-72 and water and different gaps

	FC-72[a]			Water[b]		
Gap (mm)	Measured pool boiling CHF ($W\,cm^{-2}$)	Measured pumpless loop CHF ($W\,cm^{-2}$)	Ratio of pumpless loop to pool boiling CHF	Measured pool boiling CHF ($W\,cm^{-2}$)	Measured pumpless loop CHF ($W\,cm^{-2}$)	Ratio of pumpless loop to pool boiling CHF
0.13	10.1	45.0	4.46	27.0	110.5	4.09
0.51	12.1	42.6	3.52	34.3	145.6	4.24
1.27	13.6	36.2	2.66	34.3	146.3	4.26
3.56	13.6	25.5	1.88	34.3	145.8	4.25
12.32	13.8	25.5	1.85	34.9	145.8	4.18

[a]Pool boiling CHF for FC-72 according to the Zuber et al. [8] correlation is 15.24 $W\,cm^{-2}$

[b]Pool boiling CHF for water according to the Zuber et al. [8] correlation is 110.4 $W\,cm^{-2}$

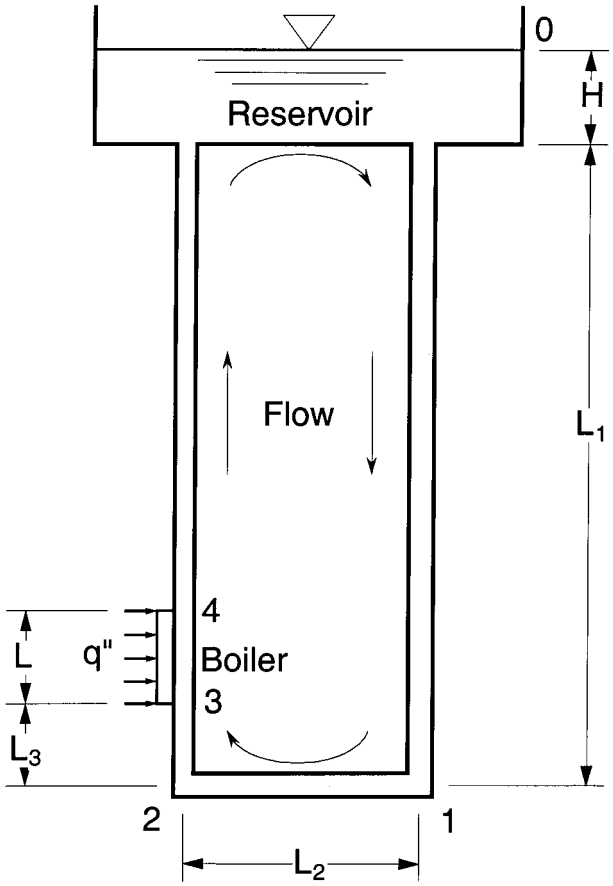

Fig. 8 Nomenclature used in pressure drop model

ing CHF data for both fluids to the pumpless loop data; also included are CHF predictions based on the Zuber et al. model [8] for pool boiling,

$$q''_m = 0.131 \rho_g h_{fg} \left[\frac{\sigma(\rho_f - \rho_g) g}{\rho_g^2} \right]^{1/4}. \tag{2}$$

Notably, the pool boiling data in the confined boiler configuration are smaller for FC-72, and much smaller for water, than predicted by the Zuber et al. model. This also implies that, for confined boilers, the present pumpless loop (a) produces great enhancement in CHF compared to pool boiling, and (b) far greater enhancement in CHF is realized with the small gaps required in miniature electronic cooling systems.

It is difficult to draw any quantitative conclusions on the effect of flow gap on CHF without understanding the various forces influencing the liquid flow into the boiler. The next section will explore this issue using a pressure drop model of the entire flow loop.

Pressure Drop Model. Figure 8 shows the nomenclature adopted in the pumpless loop model. Pressure drop in this system is comprised of frictional, accelerational, and gravitational components; accelerational effects are only encountered in the boiler, where phase change takes place. Several assumptions are used in the model, including negligible pressure losses due to the tube bends as well as the boiling module and reservoir inlet and exit effects.

Starting with a constant datum pressure P_0, corresponding to the free liquid surface in the reservoir, the pressure drops between points 0 and 1 can be represented as follows:

$$P_0 - P_1 = \Delta P_{F,0\to1} - \rho_f g (H + L_1), \tag{3}$$

$$P_1 - P_2 = \Delta P_{F,1\to2}, \tag{4}$$

$$P_2 - P_3 = \Delta P_{F,2\to3} + \rho_f g L_3, \tag{5}$$

$$P_3 - P_4 = \Delta P_{F,3\to4} + \Delta P_{A,3\to4} + \Delta P_{G,3\to4}, \tag{6}$$

$$P_4 - P_0 = \Delta P_{F,4\to0} + \Delta P_{G,4\to0}. \tag{7}$$

Adding Eqs. (3)–(7), and rearranging,

$$\Delta P_* = \rho_f g (H + L_1 - L_3) = (\Delta P_{F,0\to1} + \Delta P_{F,1\to2} + \Delta P_{F,2\to3}) + \Delta P_{F,3\to4} + \Delta P_{F,4\to0} + \Delta P_{A,3\to4} + \Delta P_{G,3\to4} + \Delta P_{G,4\to0}. \tag{8}$$

The left-hand-side term of Eq. (8) is the total pressure drop due to the liquid head only, which has to balance the two-phase gravitational and accelerational pressure drops in additional to the frictional pressure drops across the entire loop.

Frictional Pressure Drop. The frictional pressure drops resulting from single-phase flow at flow rate $\dot{m}$ inside the plastic tubing of diameter d can be combined into one term,

$$\Delta P_{F,0\to1} + \Delta P_{F,1\to2} + \Delta P_{F,2\to3} = f \left[\frac{\rho_f}{2} \right] \left[\frac{\dot{m}}{\rho_f \frac{\pi d^2}{4}} \right]^2 \left[\frac{L_1 + L_2 + L_3}{d} \right], \tag{9a}$$

where [11]

$$f = \frac{64}{\mathrm{Re}_d} \quad \text{for } \mathrm{Re}_d < 2000, \tag{9b}$$

$$f = 0.316\, \mathrm{Re}_d^{-1/4} \quad \text{for } 2000 < \mathrm{Re}_d < 2\times10^4, \tag{9c}$$

$$f = [0.79 \ln \mathrm{Re}_d - 1.64]^{-2} \quad \text{for } 2\times10^4 < \mathrm{Re}_d < 5\times10^6. \tag{9d}$$

The Petukhov correlation [12], Eq. (9*d*), is actually valid for Reynolds numbers from 3000 to 5×10^6. However, it is used here only for $\mathrm{Re}_d > 2\times10^4$ since Eq. (9*c*) is better suited for the lower range of the turbulent region.

The homogeneous equilibrium model [6,13] is used to determine the two-phase frictional, accelerational, and gravitational components of pressure drop. The Drift-flux model [14] is also used to improve the accuracy in modeling the two-phase gravitational pressure drop. A key advantage of the homogeneous equilibrium model is its ability to provide analytical expressions for the two-phase pressure drop components.

There are two distinct two-phase regions in the present loop. The first is a two-phase heated region (3–4) associated with the boiler itself, which is followed by an adiabatic two-phase region (4–0). At the boiler outlet (4), the thermodynamic equilibrium quality is expressed as

$$x_L = \frac{q'' A_s}{\dot{m} h_{fg}}, \tag{10}$$

where A_s is the area of the boiling surface. Since thermodynamic equilibrium quality x is linearly dependent on distance z along the boiling surface, the two-phase frictional pressure drop across the boiler can be expressed as

$$\Delta P_{F,3\to4} = \int_3^4 \left\{ \frac{1}{2} f_{TP} \left(\frac{\dot{m}}{A_c} \right)^2 (v_f + x v_{fg}) \frac{(\pi D)}{\left(\frac{\pi D^2}{4} \right)} \right\} dz = 2\, f_{TP} v_f \left(\frac{\dot{m}}{A_c} \right)^2 \left[1 + \frac{x_L}{2} \frac{v_{fg}}{v_f} \right] \frac{L}{D}, \tag{11}$$

where A_c is the flow area associated with the boiler gap, D is the boiler's hydraulic diameter, and f_{TP} is the two-phase friction factor, which is set equal to 0.003 [13].

Since x is constant ($=x_L$) along the adiabatic two-phase region, the two-phase frictional pressure drop form 4–0 can be expressed as

$$\Delta P_{F,4\to 0}=\int_4^0\left\{\frac{1}{2}f_{TP}\left(\frac{\dot m}{\rho_f\frac{\pi d^2}{4}}\right)^2(v_f+xv_{fg})\frac{(\pi D)}{\left(\frac{\pi D^2}{4}\right)}\right\}dz$$

$$=2\,f_{TP}v_f\left(\frac{\dot m}{\rho_f\frac{\pi d^2}{4}}\right)^2\left[1+x_L\frac{v_{fg}}{v_f}\right]\left[\frac{L_1-L_3-L}{d}\right]. \tag{12}$$

Two-Phase Accelerational Pressure Drop. Since x is a linear function of distance z along the boiling surface, the accelerational pressure drop across the boiler can be expressed as

$$\Delta P_{A,3\to 4}=\left\{\left(\frac{\dot m}{A_c}\right)^2(v_f+xv_{fg})\right\}\Big|_3^4=v_{fg}\left(\frac{\dot m}{A_c}\right)^2x_L. \tag{13}$$

Two-Phase Gravitational Pressure Drop. The homogeneous equilibrium model yields the following relations for the two-phase gravitational pressure drop across the boiler (3–4) where x is linearly dependent on z, and the adiabatic section (4–0) where $x=x_L$, respectively:

$$\Delta P_{G,3\to 4}=\int_3^4\left\{\frac{g}{v_f+xv_{fg}}\right\}dz=\frac{gL}{v_{fg}x_L}\ln\left\{1+x_L\frac{v_{fg}}{v_f}\right\}, \tag{14}$$

$$\Delta P_{G,4\to 0}=\int_4^0\left\{\frac{g}{v_f+xv_{fg}}\right\}dz=\frac{g(H+L_1-L_3-L)}{v_f+x_Lv_{fg}}. \tag{15}$$

One weakness in the homogeneous equilibrium model is its inability to account for velocity differences between the two phases. The drift-flux model represents a more powerful method to accounting for these velocity differences based on a more accurate determination of void fraction. It is also well suited for modeling the adiabatic two-phase region (4–0), where slug flow was observed exiting the boiler.

According to the homogeneous equilibrium model, the void fraction α in the two-phase adiabatic region can be related directly to the thermodynamic equilibrium quality by assuming equal phase velocities. Applying the two-phase mixture density relation

$$\overline{\rho}=\alpha\rho_g+(1-\alpha)\rho_f=\frac{1}{xv_g+(1-x)v_f} \tag{16}$$

yields the following expression for void fraction:

$$\alpha=\frac{1}{\left[1+\frac{\rho_g}{\rho_f}\left(\frac{1-x}{x}\right)\right]}, \tag{17}$$

which can be combined with Eq. (10) to express void fraction from 4 to 0 in terms of the boiler heat flux,

$$\alpha_L=\frac{1}{\left[\frac{\rho_g}{\rho_f}\frac{\dot m h_{fg}}{q''A_s}+\frac{\rho_f-\rho_g}{\rho_f}\right]}. \tag{18}$$

The drift-flux model, on the other hand, relies on flow area averaging of phase velocities and void fraction to determine an average void fraction $\langle\alpha_L\rangle$ which can be used to more accurately calculate the gravitational pressure drop from 4 to 0,

$$\Delta P_{G,4\to 0}=[\langle\alpha_L\rangle\rho_g+(1-\langle\alpha_L\rangle)\rho_f](H+L_1-L_3-L). \tag{19}$$

The average void fraction $\langle\alpha_L\rangle$ is a function of volumetric flow fraction $\langle\beta\rangle$, superficial velocity $\langle j\rangle$, weighted-mean drift-flux velocity U_{gj}, and distribution parameter C_0; the last two are dictated by the two-phase flow pattern [14],

$$\langle\alpha_L\rangle=\frac{\langle\beta\rangle}{C_0+\frac{U_{gj}}{\langle j\rangle}}, \tag{20}$$

where

$$\langle\beta\rangle=\frac{\frac{x_L\dot m}{\rho_g}}{\frac{x_L\dot m}{\rho_g}+\frac{(1-x_L)\dot m}{\rho_f}}, \tag{21}$$

$$\langle j\rangle=\frac{\frac{x_L\dot m}{\rho_g}+\frac{(1-x_L)\dot m}{\rho_f}}{A_c}, \tag{22}$$

for slug flow $C_0=1.2$, and

$$U_{gj}=0.35\left[\frac{g(\rho_f-\rho_g)d}{\rho_f}\right]^{1/2}. \tag{23}$$

Equation (8) was used to ascertain the effects of boiler gap on the various components of pressure drop for each fluid. The parameters examined include the thermodynamic equilibrium quality at the boiler exit, x_L, the void fraction at the module exit, α_L, the mass flow rate induced in the loop, $\dot m$, the liquid velocity at the inlet to the boiling surface, u_{in} ($=\dot m/(\rho_f A_c)$), and the velocity of the two-phase mixture exiting the boiling surface, u_L, which is given by

$$u_L=\left(\frac{\dot m}{A_c}\right)(v_f+x_Lv_{fg}). \tag{24}$$

The loop performance calculations were repeated for different boiler heat flux levels under saturated conditions corresponding to one atmosphere. Equation (19) was used instead of Eq. (15) to determine the gravitational pressure drop between 4 and 0.

Figures 9(a) and (b) show the pressure drop model predictions for FC-72 and water, respectively, corresponding to measured CHF for each gap and fluid. Variations of the key parameters can be clearly referenced to trends in the CHF data, which are provided in the bottom plot of each figure. Some of the predicted trends are shared by both FC-72 and water. The thermodynamic equilibrium quality and void fraction are fairly constant for large gaps but increase appreciably for small gaps. The coolant flow rate $\dot m$ is fairly constant for large gaps but decreases sharply for gaps below 4 mm for both fluids, which lends credence to the suitability of the pumpless loop to miniature electronic cooling systems demanding low coolant inventory. The liquid velocity at the inlet to the boiling surface, u_{in}, first increases with decreasing gap, reaching a maximum at about 2 mm for both FC-72 and water, below which liquid velocity decreases in accordance with the decrease in mass flow rate. The two-phase velocity at the exit of the boiling surface, u_L, shows a monotonic increase with decreasing gap culminating in very large velocities for the smallest.

Figures 9(a) and (b) also show that significant changes in pressure drop components begin to occur in concert with the large increases in void fraction and thermodynamic equilibrium quality. For both FC-72 and water, decreasing the gap increases the accelerational pressure drop across the boiling surface, and for FC-72, the frictional pressure drop. At the peak point in the accelerational pressure gradient, corresponding to about 0.50 mm for both FC-72 and water, the accelerational pressure gradient completely dominates the total pressure drop ΔP, and Eqs. (8) and (13) can be combined to yield the following approximation:

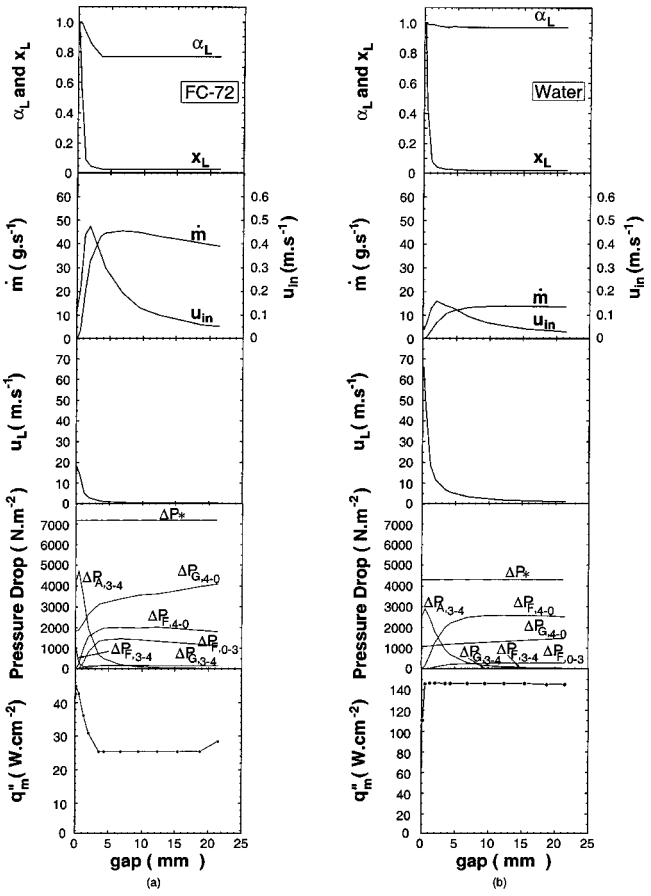

Fig. 9 Pressure drop model predictions for (*a*) FC-72 and (*b*) water

$$v_{fg}\left(\frac{\dot{m}}{A_c}\right)^2 x_L = \rho_f g(H + L_1 - L_3). \tag{25}$$

Introducing the definition of thermodynamic equilibrium quality, Eq. (10), and recalling that $A_c = L.\delta$ and $A_s = L^2$, reduce Eq. (25) to

$$\dot{m} = \left\{\frac{\rho_f g h_{fg}(H + L_1 - L_3)}{v_{fg}}\right\}\frac{\delta^2}{q''_m}. \tag{26}$$

Thus the loop's mass flow rate for small gaps is proportional to the square of the gap and inversely proportional to CHF.

Figures 9(*a*) and (*b*) clearly illustrate two key advantages of a smaller gap: (a) small coolant inventory requirements, and (b) enhanced CHF due to high acceleration of the two-phase mixture across the boiling surface. Since the pressure drop model does not account for blockage of the replenishment liquid in the case of water, it can be concluded that the model is valid for FC-72 but not for water. In other words, the growth of large bubbles in water will cause virtually complete blockage of the flow, greatly reducing the liquid flow rate and two-phase mixture velocity for water compared to the model predictions.

Conclusions

This paper explored a pumpless cooling system specifically tailored to compact, high-flux electronic cooling systems. Experiments were performed on a flat vertical boiling surface with water and FC-72 using different boiler gaps. A pressure drop model was constructed to determine how the gap influences the various forces in the system, and hence system response to heat input. Below are the key findings from the study.

1. Like pool boiling thermosyphons, the present system is self-sustaining and relies on density differences to ensure liquid replenishment of the boiling surface during severe boiling. But unlike pool boiling thermosyphons, the pumpless loop completely isolates the path of the replenishment liquid from that of the vapor exiting the boiler.
2. The pumpless loop completely eliminates the incipient boiling temperature drop common to low contact angle coolants and reduces overall thermal cycling to negligible levels.
3. While pool boiling in small gaps greatly reduces CHF compared to an infinite liquid pool, small gaps actually increase CHF with the pumpless loop. CHF multiples as high as 4.5 and 4.2 were realized relative to pool boiling with identical gaps for FC-72 and water, respectively.
4. For both fluids, CHF shows little dependence on boiler gap for large gaps. However, small gaps produce CHF variations that are both drastic and follow opposite trends for the two fluids. Decreasing the gap below 3.56 mm produces a substantial rise in CHF for FC-72. For water, CHF is fairly insensitive down to 0.51 mm, below which it begins to decrease sharply.
5. The CHF trends with boiler gap are closely related to the small surface tension and contact angle of FC-72 greatly reducing bubble departure diameter. Very small bubbles can therefore be passed through narrow gaps in FC-72, while much larger bubbles obstruct liquid replenishment in narrow gaps for water.
6. Small gaps cause large increases in the accelerational and, to a lesser extent, frictional pressure components of pressure drop across the boiler itself in FC-72. High CHF is possible with small gaps due to the large acceleration of the two-phase mixture across the boiling surface. The same effect is not possible in water due to the blockage caused by large bubbles.

Acknowledgment

The authors are grateful for the support of the Office of Basic Energy Sciences of the U.S. Department of Energy (Award No. DE-FG02-93ER14394 A7).

Nomenclature

A_c = Flow area associated with boiler gap adjacent to boiling surface, $\delta.L$
A_s = Heated area of boiling surface, L^2
Bo = Bond number defined in Eq. (1)
C_0 = Drift-flux distribution parameter
D = Hydraulic diameter associated with boiler gap adjacent to boiling surface, $4A_c/p$
d = Inner diameter of tubing used in cooling loop
d_b = Bubble departure diameter
f = Single-phase friction factor
f_{TP} = Two-phase friction factor
g = Acceleration due to gravity
H = Height of liquid in reservoir
h_{fg} = Latent heat of vaporization
$\langle j \rangle$ = Superficial velocity defined in Eq. (22)
L = Square dimension of boiling surface
L_1, L_2, L_3 = Lengths of tubing sections indicated in Fig. 8
$\dot{m}$ = Mass flow rate induced in loop
P = Pressure
p = Perimeter of boiler gap, $2(L + \delta)$
ΔP = Pressure drop
ΔP_* = Total pressure drop due to liquid head alone
ΔP_A = Accelerational pressure drop
ΔP_F = Frictional pressure drop
ΔP_G = Gravitational pressure drop
q'' = Heat flux
q''_m = Critical heat flux

Re_d = Reynolds number associated with liquid flow in tubing, $4\dot{m}/(\pi d\mu_f)$
T = Temperature
u_{in} = Liquid velocity at inlet to boiling surface
u_L = Two-phase mixture velocity at exit from boiling surface
U_{gj} = Weighted-mean drift velocity defined in Eq. (23)
v = Specific volume
v_{fg} = Specific volume difference between vapor and liquid
x = Thermodynamic equilibrium quality
x_L = Thermodynamic equilibrium quality at exit from boiling surface

Greek symbols

α = Void fraction
α_L = Void fraction at exit from boiling surface
$\langle\alpha\rangle$ = Area-weighted void fraction
$\langle\beta\rangle$ = Area-weighted volumetric flow fraction defined in Eq. (21)
δ = Gap thickness
θ = Contact angle
ρ = Density
σ = Surface tension

Subscripts

0,1,2,3,4 = Reference points in cooling loop defined in Fig. 8
f = Liquid
fg = Difference between vapor and liquid
g = Vapor
$i\rightarrow j$ = Between points i and j, $i=0-4$, $j=0-4$
in = Inlet to boiling surface
L = Exit from boiling surface (point 4 in Fig. 8)
m = Maximum, CHF condition
out = Exit from boiling surface
sat = Saturation
w = Wall
z = Distance along direction of fluid flow

References

[1] Mudawar, I., 2001, ''Assessment of High-Heat-Flux Thermal Management Schemes,'' IEEE Trans. Compon., Packag. Manuf. Technol., Part A, **24**, pp. 122–141.
[2] Boyd, R. D., 1985, ''Subcooled Flow Boiling Critical Heat Flux (CHF) and its Application to Fusion Energy Components—Part I. A Review of Fundamentals of CHF and Related Data Base,'' Fusion Technol., **7**, pp. 7–31.
[3] Mudawar, I., and Bowers, M. B., 1999, ''Ultra-High Critical Heat Flux (CHF) for Subcooled Water Flow Boiling—I. CHF Data and Parametric Effects for Small Diameter Tubes,'' Int. J. Heat Mass Transfer, **42**, pp. 1405–1428.
[4] Rogers, C. S., Mills, D. M., Lee, W. K., Knapp, G. S., Holmberg, J., Freund, A., Wulff, M., Rossat, M., Hanfland, M., and Yamaoka, H., 1995, ''Performance of a Liquid-Nitrogen-Cooled, Thin Silicon Crystal Monochromator on a High-Power, Focussed Wiggler Synchrotron Beam,'' Rev. Sci. Instrum., **66**, pp. 3494–3499.
[5] Tuckerman, D. B., and Pease, R. F. W., 1981, ''High-Performance Heat Sinking for VLSI,'' IEEE Electron Device Lett., **EDL-2**, pp. 126–129.
[6] Bowers, M. B., and Mudawar, I., 1994, ''High Flux Boiling in Low Flow Rate, Low Pressure Drop Mini-Channel and Micro-Channel Heat Sinks,'' Int. J. Heat Mass Transfer, **37**, pp. 321–332.
[7] Anderson, T. M., and Mudawar, I., 1989, ''Microelectronic Cooling by Enhanced Pool Boiling of a Dielectric Fluorocarbon Liquid,'' ASME J. Heat Transfer, **111**, pp. 752–759.
[8] Zuber, N., Tribus, M., and Westwater, J. W., 1961, ''The Hydrodynamic Crisis in Pool Boiling of Saturated and Subcooled Liquids,'' *Int. Dev. Heat Transfer: Proc. 1961-62 Int. Heat Transfer Conf.*, Boulder, CO, pp. 230–236.
[9] Bergles, A. E., Collier, J. G., Delhaye, J. M., Hewitt, G. F., and Mayinger, F., 1981, *Two-Phase Flow and Heat Transfer in the Power and Process Industries*, Hemisphere Publishing Corp., New York.
[10] Fritz, W., 1935, ''Berechnung des Maximalvolume von Dampfblasen,'' Phys. Z., **36**, pp. 379–388.
[11] Incropera, F. P., and Dewitt, D. P., 1996, *Fundamentals of Heat and Mass Transfer*, 4th Ed., John Wiley and Sons, New York.
[12] Petukhov, B. S., 1970, in *Advances in Heat Transfer*, T. F. Irvine and J. P. Hartnett, Eds., Vol. 6, Academic Press, New York.
[13] Collier, J. G., 1981, *Convective Boiling and Condensation*, McGraw-Hill, London.
[14] Zuber, N., and Findlay, J. A., 1965, ''Average Volumetric Concentration in Two-Phase Flow Systems,'' ASME J. Heat Transfer, **87**, pp. 453–468.